OVERVIEW OF PHENIX EXPERIMENT AT RHIC*

Susumu Sato

for the PHENIX Collaboration

Japan Atomic Energy Agency (JAEA)/RIKEN, Japan

Received 31 March 2026, accepted 20 May 2026, published online 10 July 2026

The Relativistic Heavy Ion Collider (RHIC) at Brookhaven National Laboratory (BNL) has been operated since 2001, contributing significantly to the study of strong interactions described by QCD and of nuclear matter under extreme conditions. The PHENIX experiment has collected a comprehensive dataset and continues to publish scientific papers, yielding impactful insights from the initial to final stages of nucleus collisions. Recently published results advance our understanding of strong interactions and nuclear matter.

DOI:10.5506/APhysPolBSupp.19.4-A26

1. Introduction

The RHIC has been contributing significantly to the study of strong interactions described by QCD and of nuclear matter under extreme conditions. The PHENIX experiment at RHIC, operated from 2001 to 2016, has collected a comprehensive dataset (see Fig. 1) and continues to publish scientific papers, yielding impactful results from the initial to final stages of nucleus collisions. These measurements have provided critical insights into the properties of the quark–gluon plasma (QGP) and cold nuclear matter (CNM) which also affect small collision systems.

Some of selected observations from recent publications are overviewed here; first, for particle-identified hadrons, second for heavy-flavor probes, and third for electromagnetic probes. The direct photon yield shows many interesting features. These observations highlight ongoing contributions of the PHENIX experiment in both soft and hard sectors.

* Presented at the Excited QCD 2026 Workshop, Granada, Spain, 8–14 January, 2026.

$\sqrt{s_{NN}}$ [GeV]	pp	pAl	pAu	dAu	HeAu	CuCu	CuAu	AuAu	UU
510	o								
200	o	o	o	o	o	o	o	o	o
130								o	
62.4	o			o		o		o	
39				o				o	
27								o	
20				o		o		o	
14.5								o	
7.7								o	

Fig. 1. Summary of the PHENIX collision systems.

2. PHENIX experimental setups

The PHENIX experiment [1, 2] included several subdetectors that are grouped into four main blocks called arms. The central arms (east and west) [3] cover midrapidity ($|\eta| < 0.35$) and are intended for measurement of electrons, photons, and charged hadrons with PID [4, 5]. The muon arms (south and north) [6] and silicon detectors [7] cover forward and backward ($1.2 < |\eta| < 2.2$) rapidity. Figure 2 shows an overview of the PHENIX experimental setup.

3. Particle-identified hadron

Systematic measurements for identified charged hadrons, namely invariant p_{T} spectra, nuclear-modification factors (called R_{AA}), and particle ratios have been done in $p + \mathrm{Al}$, $^3\mathrm{He} + \mathrm{Au}$, and $\mathrm{Cu} + \mathrm{Au}$ collisions at $\sqrt{s_{NN}} = 200$ GeV and in $\mathrm{U} + \mathrm{U}$ collisions at $\sqrt{s_{NN}} = 193$ GeV [8]. Figure 3 shows invariant p_{T} spectra of identified charged hadrons in these collisions ([8], Fig. 3).

The values of freeze-out temperatures and average collective velocities have been obtained. These values advance our understanding of strong interactions described by QCD and nuclear matter. Strangeness production and π^0 productions in various collision systems are also of great importance.

3.1. Freeze-out temperature

The π, K, and p invariant p_{T} spectra exhibit different shapes. To quantify these differences, invariant-transverse mass ($m_{\mathrm{T}} = \sqrt{p_{\mathrm{T}}^2 + m_0^2}$) spectra were calculated. The m_{T} invariant spectra of all identified charged hadrons have an exponential form for $m_{\mathrm{T}} < 1.5$ GeV and can be approximated by

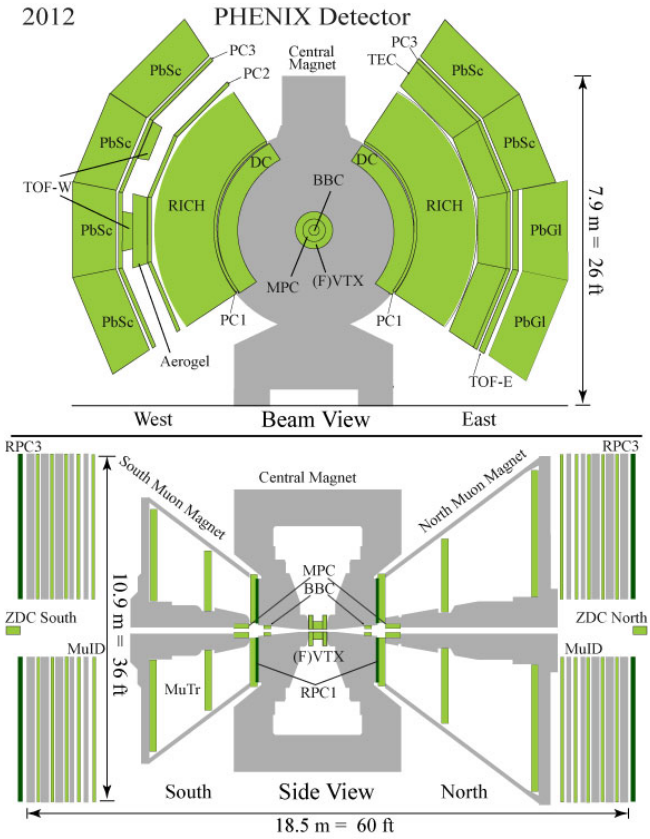

Fig. 2. Overview of the PHENIX experimental setup.

$$\frac{1}{2\pi m_{\mathrm{T}}}\frac{\mathrm{d}^2N}{\mathrm{d}m_{\mathrm{T}}\mathrm{d}y} = \frac{A}{2\pi T\left(T+m_0\right)}\exp\left(-\frac{m_{\mathrm{T}}-m_0}{T}\right), \tag{1}$$

where y is the rapidity, T is the inverse-slope parameter and A is a normalization factor. Thermal models consider a thermalized system with a well-defined temperature and a common transverse velocity field. Under the assumption of complete decoupling between the thermal and collective motion of the particles, the hadron kinetic energy ($\langle E_{\mathrm{kinetic}}\rangle$) is equal to the linear sum of the energy of the thermal motion ($\langle E_{\mathrm{thermal}}\rangle$) and the energy of the collective motion ($\langle E_{\mathrm{collective}}\rangle$), $\langle E_{\mathrm{kinetic}}\rangle = \langle E_{\mathrm{thermal}}\rangle + \langle E_{\mathrm{collective}}\rangle$. The T exhibits mass dependence given by $T = T_0 + m\langle u_t\rangle^2$, where T_0 can be interpreted as a freeze-out temperature and $\langle u_t\rangle$ as the average collective velocity for all particle species. The averaged T_0 value was found to be 166.1 $\pm$ 2.2 MeV ([8], Fig. 6).

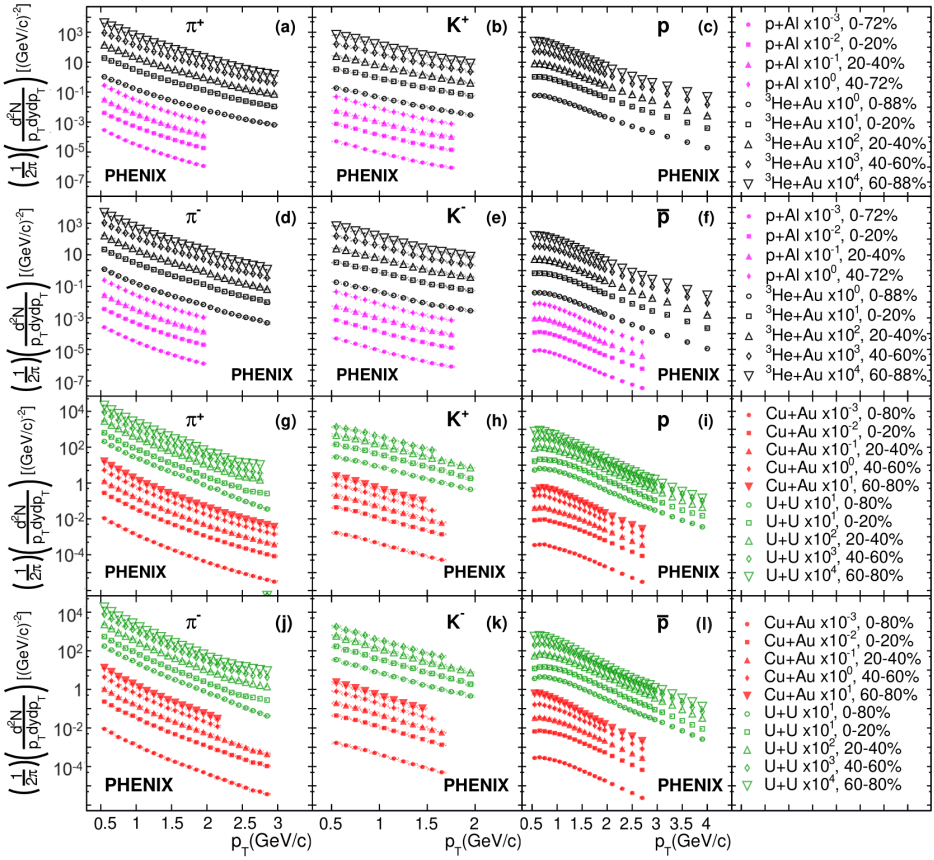

Fig. 3. Invariant p_{T} spectra of identified charged hadron s in $p + \mathrm{Al}$, $^3\mathrm{He} + \mathrm{Au}$, and $\mathrm{Cu} + \mathrm{Au}$ collisions at $\sqrt{s_{NN}} = 200$ GeV and in $\mathrm{U} + \mathrm{U}$ collisions at $\sqrt{s_{NN}} = 193$ GeV [8].

3.2. Strangeness enhancement at forward rapidity

We have measured the production of $\omega + \rho$ and ϕ mesons at forward and backward rapidities via the $\mu^+\mu^-$ decay channel in $p + p$ and $\mathrm{Au} + \mathrm{Au}$ collisions at $\sqrt{s_{NN}} = 200$ GeV. This study represents the first measurement of the invariant yields and nuclear-modification factors for $\omega + \rho$ and ϕ mesons in $\mathrm{Au} + \mathrm{Au}$ collisions at RHIC in the forward/backward rapidity regions. The results are presented as a function of N_{part} and p_{T}.

The flavor dependence of medium effects is examined by comparing the R_{AA} of the ϕ, $\omega + \rho$, and J/Ψ mesons.

Both $\omega + \rho$ and J/Ψ mesons exhibit suppression across the entire p_{T} range, although their p_{T} dependence differs slightly. Their behavior as a function of N_{part} is generally similar, except in peripheral collisions, where

they diverge. In contrast, the strange flavor (ϕ meson) shows a distinct pattern, with enhancement ([9], Figs. 13, 14) observed at intermediate values of both p_{T} and N_{part}.

3.3. Neutral pion R_{AA} with the "experimental" N_{coll}

Empirically, the number of binary collisions ($N_{\mathrm{coll}}^{\mathrm{EXP}}$) for a given event selection is estimated from the ratio of the direct-photon yields in that selection to the yield from $p+p$ collisions ([10])

$$N_{\mathrm{coll}}^{\mathrm{EXP}}(p_{\mathrm{T}}) = \frac{Y_{\mathrm{dAu}}^{\gamma^{\mathrm{dir}}}(p_{\mathrm{T}})}{Y_{pp}^{\gamma^{\mathrm{dir}}}(p_{\mathrm{T}})}\,. \tag{2}$$

Next, possible nuclear modifications of π^0 production in $d+\mathrm{Au}$ collisions with high event activity (evaluated by the charged particle multiplicity measured by the minimum-bias trigger counter [11]) are investigated ([10], Fig. 3). For this purpose, the nuclear modification factor ($R_{\mathrm{dAu,EXP}}^{\pi^0}$) is calculated using $N_{\mathrm{coll}}^{\mathrm{EXP}}$ (as defined in Eq. (3), instead of $N_{\mathrm{coll}}^{\mathrm{Glauber}}$ [12, 13])

$$R_{\mathrm{dAu,EXP}}^{\pi^0} = \frac{Y_{\mathrm{dAu}}^{\pi^0}}{N_{\mathrm{coll}}^{\mathrm{EXP}} Y_{pp}^{\pi^0}} = \frac{Y_{pp}^{\gamma^{\mathrm{dir}}}/Y_{pp}^{\pi^0}}{Y_{\mathrm{dAu}}^{\gamma^{\mathrm{dir}}}/Y_{\mathrm{dAu}}^{\pi^0}} \tag{3}$$

which is equivalent to the double ratio of $\gamma^{\mathrm{dir}}/\pi^0$ ratios.

A further ratio of the averaged nuclear modification factor ($R_{\mathrm{dAu,EXP}}^{\pi^0}$) for the highest event activity (0%–5%) samples and the factor for the whole event activity (0%–100%) samples is evaluated as

$$\frac{R_{\mathrm{dAu,EXP}}^{\pi^0}(0\%\text{–}5\%)}{R_{\mathrm{dAu,EXP}}^{\pi^0}(0\%\text{–}100\%)} = 0.806 \pm 0.042 \tag{4}$$

which corresponds to a 4.5σ deviation from unity. The same ratio for events with the smallest event activity is 1.017 ± 0.056, consistent with unity.

The $N_{\mathrm{coll}}^{\mathrm{EXP}}$ based on direct photons provides a more accurate approximation of the hard-scattering contribution to the neutral pion production. Using $N_{\mathrm{coll}}^{\mathrm{EXP}}$ eliminates the enhancement in low activity events, while maintaining a 20% suppression of high p_{T} π^0 in events with high activity. The observed suppression is qualitatively consistent with the predictions of energy loss in small systems.

4. Heavy flavor

The magnitudes of elliptic flow (the coefficient is called v_2) measured by the PHENIX muon arms ($1.2 < |\eta| < 2.0$) for charged hadrons ([14], Fig. 10) and open-heavy-flavor muons ([14], Fig. 11), are compared as a function of p_{T}. The results are also compared to previous PHENIX measurements ([15]) at midrapidity ($|\eta| < 0.35$).

The v_2 ([14], Fig. 11) of open-heavy-flavor muons at forward rapidity is directly compared to that of charged hadrons in the same rapidity range, and to the v_2 of open-heavy-flavor electrons at midrapidity as previous PHENIX results ([16]).

The heavy-flavor muons exhibit smaller v_2 than the light hadrons, as expected, given the mass ordering of particle interactions with the QGP.

5. Direct photon production with high statistics data

The measurement of the direct-photon spectrum in Au + Au collisions at $\sqrt{s_{NN}} = 200$ GeV, is successfully performed by the PHENIX Collaboration using the external photon-conversion technique ([17]). Also, the direct photon enhancements are qualitatively discussed. The nonprompt direct-photon spectra are isolated by subtracting the prompt-photon contribution ([17], Figs. 15, 16), which is estimated through a fit to the direct-photon data from $p + p$ collisions at $\sqrt{s} = 200$ GeV, measured by PHENIX.

In the lower p_{T} range from 0.8 to 1.9 GeV/c, the spectra are well described by $T_{\mathrm{eff}} = 0.26$ GeV/c ([17], Fig. 18). This is consistent with what is expected for radiation from the late QGP stage until freeze-out. Above a p_{T} of 2 GeV/c, the inverse slope of the spectra continues to increase with p_{T}. Between $p_{\mathrm{T}} = 2$ and 4 GeV/c, the average inverse slope is $T_{\mathrm{eff}} \approx 0.376$ GeV/c ([17], Fig. 18). This T_{eff} is larger than what model calculations for a rapidly expanding hadron gas can accommodate, thus suggesting that emissions from the QGP phase and earlier times in the evolution start to dominate the spectra.

REFERENCES

[1] PHENIX Collaboration (K. Adcox *et al.*), *Nucl. Instrum. Methods Phys. Res. A* **499**, 469 (2003).

[2] PHENIX Collaboration (M. Allen *et al.*), *Nucl. Instrum. Methods Phys. Res. A* **499**, 549 (2003).

[3] PHENIX Collaboration (K. Adcox *et al.*), *Nucl. Instrum. Methods Phys. Res. A* **499**, 489 (2003).

[4] L. Carlén *et al.*, *Nucl. Instrum. Methods Phys. Res. A* **431**, 123 (1999).

[5] PHENIX Collaboration (M. Aizawa *et al.*), *Nucl. Instrum. Methods Phys. Res. A* **499**, 508 (2003).

[6] H. Akikawa *et al.*, *Nucl. Instrum. Methods Phys. Res. A* **499**, 537 (2003).

[7] C. Aidala *et al.*, *Nucl. Instrum. Methods Phys. Res. A* **755**, 44 (2014).

[8] PHENIX Collaboration (N.J. Abdulameer *et al.*), *Phys. Rev. C* **109**, 054910 (2024), arXiv:2312.09827 [nucl-ex].

[9] PHENIX Collaboration (N.J. Abdulameer *et al.*), *Phys. Rev. C* **112**, 064918 (2025).

[10] PHENIX Collaboration (N.J. Abdulameer *et al.*), *Phys. Rev. Lett.* **134**, 022302 (2025).

[11] M. Allen *et al.*, *Nucl. Instrum. Methods Phys. Res. A* **499**, 549 (2003).

[12] R.J. Glauber, G. Matthiae, *Nucl. Phys. B* **21**, 135 (1970).

[13] M.L. Miller, K. Reygers, S.J. Sanders, P. Steinberg, *Annu. Rev. Nucl. Part. Sci.* **57**, 205 (2007).

[14] PHENIX Collaboration (N.J. Abdulameer *et al.*), *Phys. Rev. C* **112**, 034902 (2025).

[15] PHENIX Collaboration (A. Adare *et al.*), *Phys. Rev. C* **92**, 034913 (2015).

[16] PHENIX Collaboration (A. Adare *et al.*), *Phys. Rev. Lett.* **98**, 172301 (2007).

[17] PHENIX Collaboration (N.J. Abdulameer *et al.*), *Phys. Rev. C* **109**, 044912 (2024).